Available online at www.sciencedirect.com
SCIENCE DIRECT®
Wave Motion 40 (2004) 263–276
WAVE MOTION
www.elsevier.com/locate/wavemoti

An FE-FCT method with implicit functions for the study of shock wave propagation in solids

Shaoping Xiao*

Department of Mechanical and Industrial Engineering and Center for Computer-Aided Design, The University of Iowa, 3131 Seamans Center, Iowa City, IA 52242, USA

Received 2 February 2004; accepted 8 April 2004

Available online 28 May 2004

Abstract

A finite element flux-corrected transport (FE-FCT) method is proposed for the study of shock wave propagation in solids. The FCT algorithm contains two stages: transport and antidiffusion. The total Lagrangian finite element method is used here and the FCT algorithm is only applied to correct the nodal velocities along the lines of the structured mesh. An implicit function is implemented into the finite element method so that the objective with arbitrary boundaries can be modeled with structured mesh. Both one-dimensional and two-dimensional examples show that the FE-FCT method can efficiently eliminate the oscillations behind the shock wave fronts.

Keywords: Flux-corrected transport; Finite element; Implicit function

1. Introduction

The study of shock wave propagation in solids will improve our understanding of material response under the situations of high pressures, high temperatures and very short times [1–3]. Numerical methods, especially finite element (FE) methods [4], have become powerful tools to elucidate the complex mechanical and physical phenomena. However, most of them have difficulties to simulate shock wave propagation problems since oscillations are always observed behind the shock wave fronts. In this paper, a new method is proposed and it can be used to accurately describe the shock wave propagation in solids.

One of the common techniques to reduce the oscillations behind the shock wave fronts is artificial bulk viscosity [5]. It can efficiently eliminate the oscillations but the shock wave fronts are observed to be spread over several elements or space step sizes if FE methods or finite difference (FD) methods are used, respectively. Moreover, the total energy of the system somewhat dissipates due to the artificial bulk viscosity. It has been shown that the flux-corrected transport (FCT) can perfectly solve the above issues. The FCT algorithm was first proposed by Boris and Book [6,7] in 1970s. This algorithm consists of two stages: the transport stage and the antidiffusion stage. The antidiffusion stage is a corrective stage which corrects numerical errors introduced in the transport stage. Both

* Tel.: +1-319-3356009; fax: +1-319-3355669.
E-mail address: shaoping-xiao@uiowa.edu (S. Xiao).

0165-2125/$ – see front matter © 2004 Elsevier B.V. All rights reserved.
doi:10.1016/j.wavemoti.2004.04.002

stages are conservative and positive. Their interaction enables the FCT algorithm to treat discontinuities without the usual dispersively generated ripples (oscillations). It has been applied in different schemes of the FD methods [7], and good results were obtained for the shock test problems [6] in fluids. Zalesak [8] described the FCT algorithm in details and extended this algorithm to the multidimensional problems. In his multidimensional FCT technique, a low order monotonic scheme and a high order scheme are needed. The FCT algorithm has been developed and applied in some research areas [9–11] and it still has potential.

Since the FE methods have been well developed today and widely used to solve many complex physical and mechanical problems. Some researchers try to implement the FCT algorithm into the FE methods [12–15]. Löhner et al. [12] combined the FCT algorithm with the Eulerian FE methods and obtained good results for Navier–Stokes equations. Then, they proposed a general Eulerian finite element flux-corrected transport (FEM-FCT) algorithm on unstructured grids [13]. In their method, the high order solution is used in smooth regions of the problems and the low order solution is used for the discontinuities such as shock wave fronts. Georghiou et al. [14] developed a similar two-dimensional FEM-FCT method which contains a low order positive ripple-free scheme and a high order scheme. The above developments are mainly for the studies of shocks in fluids. Since the FE methods based on the Lagrangian description are usually used in solid mechanics, the implementation of the FCT algorithm into Lagrangian FE method, especially the total Lagrangian FE method [15], will result in a powerful tool to study the shock wave propagation in solids. Zhang et al. [16] successfully coupled the FCT algorithm and the Lagrangian finite element method together, and they obtained some interesting results in one dimension.

A new finite element flux-correction transport (FE-FCT) method is proposed in this paper. The FCT algorithm used here is from the fundamental version proposed by Boris et al. [6,7]. The discrete equations of motion in FE methods can be viewed as the partial different equations (PDEs), which need to be corrected by the FCT algorithm. Once structured meshes are generated, each component of the nodal velocities is corrected separately within each time step. It is simpler than FD methods because the FCT algorithm needs to apply on each PDE. Moreover, the proposed FE-FCT method does not require low order and high order scheme as the previous ones [13,14]. However, the requirement for structured meshes will be an issue when an objective with arbitrary boundaries is considered. To solve this issue, the method is linked to the extended finite element method [17,18]. An implicit function is introduced to describe the boundaries of the objective. This enables the modeling to include features such as boundaries that are not coincident with the mesh. Therefore, the proposed FE-FCT method can be easily applied to two-dimensional solid problems and the stable, non-oscillatory results are observed. Such an FE-FCT method for three-dimensional form is ready to go.

The outline of this paper is as follows. In Section 2, the general governing equation and the discrete equations are given. Section 3 describes the FCT algorithm first and gives a flow chart for the FE-FCT method. An implicit function is introduced to describe the arbitrary boundaries. This implicit function is implemented into the proposed FE-FCT method. Several examples including one-dimensional and two-dimensional problems are studied in Section 4, followed by the conclusions.

2. Governing equation

Here, a problem domain Ω (current configuration) with a reference configuration Ω_0 is considered. The motion is described by

$$\mathbf{x} = \phi(\mathbf{X}, t), \tag{1}$$

where $\mathbf{x}$ is the spatial (Eulerian) coordinate and $\mathbf{X}$ the material (Lagrangian) coordinate. The above map must be one-by-one except on sets of measure zero (i.e., surfaces in three-dimensional), where points are split into two to model cracking.

The momentum equations are

$$\nabla_0 \cdot \mathbf{P} + \rho_0 \mathbf{b} = \rho_0 \mathbf{u} \quad \text{or} \quad \sum_j \frac{\partial P_{ji}}{\partial X_j} + \rho_0 b_i = \rho_0 \ddot{u}_i, \tag{2}$$

where ρ_0 is the initial density, $\mathbf{P}$ the nominal stress tensor, $\mathbf{b}$ the body force, $\mathbf{u}$ the displacement, and superposed dots denote material time derivatives. (2) is used in reference configuration. When the current configuration corresponds to the reference configuration, i.e., when $\Omega_0 = \Omega$, the above form of the momentum equations can be written as the spatial form of the momentum equations:

$$\nabla \cdot \boldsymbol{\sigma} + \rho \mathbf{b} = \rho \ddot{\mathbf{u}} \quad \text{or} \quad \sum_j \frac{\partial \sigma_{ji}}{\partial x_j} + \rho b_i = \rho \ddot{u}_i, \tag{3}$$

where ρ is the current density. By conservation of mass:

$$\rho J = \rho_0, \tag{4}$$

where J is the Jacobian determinant of deformation gradient $\mathbf{F}$, which are defined by

$$J = \det(\mathbf{F}), \qquad F_{ij} = \frac{\partial x_i}{\partial X_j}. \tag{5}$$

The two above forms of momentum equations are identical and differ in form only because they are expressed in a different description; see [15]. Here, the total Lagrangian finite element method is used. Therefore, the approximation for the displacements in Lagrangian mesh is

$$\mathbf{u}^h(\mathbf{X}, t) = \mathbf{N}^{\mathrm{T}}(\mathbf{X})\mathbf{u}(t) \quad \text{or} \quad u_i^h(\mathbf{X}, t) = \sum_J N_J(\mathbf{X}) u_{iJ}(t), \tag{6}$$

where the shape function $N_J(\mathbf{X})$ is a function of the material coordinates in total Lagrangian description. The above approximation reproduces constant functions and linear functions exactly. Then, the approximation for the first derivatives of the displacement can be written as

$$\nabla_0 \mathbf{u}^h(\mathbf{X}, t) = \mathbf{B}^{\mathrm{T}}(\mathbf{X})\mathbf{u}(t) \quad \text{or} \quad \frac{\partial u_i^h(\mathbf{X}, t)}{\partial X_j} = \sum_J \frac{\partial N_J(\mathbf{X})}{\partial X_j} u_{iJ}(t). \tag{7}$$

The discrete momentum equation can be obtained by the Galerkin weak form. In reference configuration, the weak form of the linear momentum conservation equation is

$$\int_{\Omega_0} \delta u_i \rho_0 \ddot{u}_i \, \mathrm{d}\Omega_0 = \int_{\Omega_0} \delta u_i \rho_0 b_i \, \mathrm{d}\Omega_0 - \int_{\Omega_0} \sum_j \frac{\partial(\delta u_i)}{\partial X_j} P_{ji} \, \mathrm{d}\Omega_0 + \int_{\Gamma_0^t} \delta u_i \bar{t}_i \, \mathrm{d}\Gamma_0^t, \tag{8}$$

where δu_i is the test function, and $\bar{t}_i$ the boundary traction. Substituting (6) and (7) into (8) and using a diagonal mass matrix, the equations of motion can be obtained as

$$\mathbf{M}\ddot{\mathbf{u}} = \mathbf{f}^{\mathrm{ext}} - \mathbf{f}^{\mathrm{int}} \quad \text{or} \quad M_I \ddot{u}_{iI} = f_{iI}^{\mathrm{ext}} - f_{iI}^{\mathrm{int}}, \tag{9}$$

where M_I is nodal mass for node I, and f_{iI}^{ext}, f_{iI}^{int} are the external and internal nodal force, respectively, given by

$$f_{iI}^{\mathrm{ext}} = \int_{\Omega_0} \rho_0 N_I(\mathbf{X}) b_i \, \mathrm{d}\Omega_0 + \int_{\Gamma_0^t} N_I(\mathbf{X}) \bar{t}_i \, \mathrm{d}\Gamma_0^t, \tag{10}$$

$$f_{iI}^{\mathrm{int}} = \int_{\Omega_0} \sum_j \frac{\partial N_I(\mathbf{X})}{\partial X_j} P_{ji} \, \mathrm{d}\Omega_0. \tag{11}$$

3. FE-FCT method

3.1. Flux-corrected transport algorithm

FCT algorithm was first used in the FD methods [6,7]. We first consider any function U, which is a function of time and space in one-dimensional. In FD method, the value of function U at spatial step j and time step $n+1$ can be written as

$$U_j^{n+1} = f(U_j^n, \Delta t, \Delta X), \tag{12}$$

where Δt is the time-step size and ΔX the spatial increment.

Based on what Boris and Book [6] proposed, the general FCT algorithm can be expressed as follows:

(a) Transport calculation: obtaining trial values of function U at time step $n+1$ from (12):

$$\tilde{U}_j^{n+1} = f(U_j^n, \Delta t, \Delta X). \tag{13}$$

(b) Diffusive fluxes calculation:

$$\varphi_j^0 = \eta_1(U_{j+1}^n - U_j^n), \tag{14}$$

where η_1 is diffusive coefficient.

(c) Diffusion:

$$\bar{U}_j^{n+1} = \tilde{U}_j^{n+1} + \varphi_j^0 - \varphi_{j-1}^0. \tag{15}$$

(d) Antidiffusive fluxes calculation:

$$\varphi_j^1 = \eta_2(\tilde{U}_{j+1}^n - \tilde{U}_j^n), \tag{16}$$

where η_2 is antidiffusive coefficient.

(e) Limitation of antidiffusive fluxes

$$\varphi_j^C = S \max\{0, \min[S \cdot \Delta_{j-1}, |\varphi_j^1|, S \cdot \Delta_{j+1}]\}, \tag{17}$$

where $\Delta_{j-1} = \bar{U}_j^{n+1} - \bar{U}_{j-1}^{n+1}$, and $S = \text{sign}(\varphi_j^1)$.

(f) Antidiffusion:

$$U_j^{n+1} = \bar{U}_j^{n+1} - \varphi_j^C + \varphi_{j-1}^C. \tag{18}$$

In this paper, the diffusive coefficient and antidiffusive coefficient are constant, i.e. $\eta_1 = \eta_2 = 0.125$ [6,7]. When the above FCT algorithm is implemented into the FD methods, it can efficiently eliminate the oscillations behind the shock wave fronts. Let us consider a square shape velocity wave propagating in an elastic rod. The governing equations are

$$\rho \frac{\partial v}{\partial t} = \frac{\partial \sigma}{\partial x}, \tag{19}$$

$$\frac{\partial \varepsilon}{\partial t} = \frac{\partial v}{\partial x}. \tag{20}$$

Leapfrog time integration algorithm is used in this problem. Within each time step, we first obtain velocity v from (19) and apply the FCT algorithm to correct it. Then, we obtain strain ε from (20) and correct it once more by using the same FCT algorithm. Fig. 1(a) shows that the oscillations occur behind the shock wave fronts when the FD method is used without any filtering processing. However, if FCT algorithms are applied, we can obtain very good discontinuous shapes for shock wave fronts when they propagate along the media as shown in Fig. 1(b).

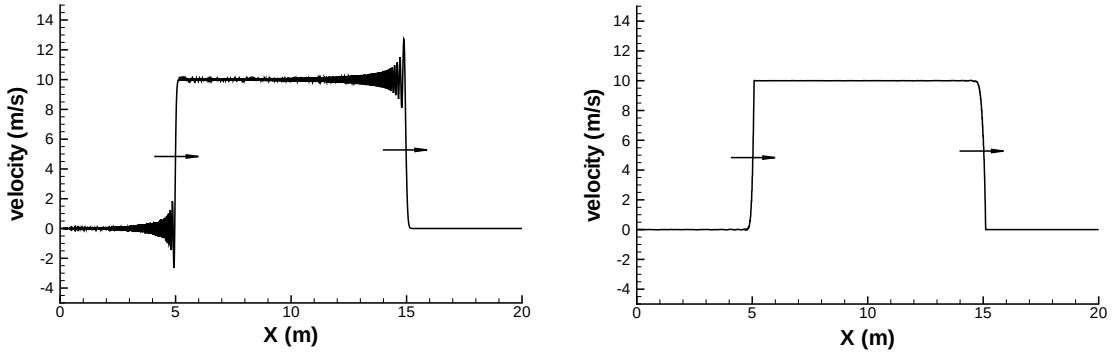

(a) FD method without FCT

(b) FD method with FCT

Fig. 1. Square shape velocity wave propagating along one-dimensional elastic rod.

3.2. A general FE-FCT method

The FD methods usually need to solve several PDEs especially in multi-dimensional problems so that the FCT algorithm needs to be applied on each PDE. The FE methods are almost well developed today and it has been widely used to solve a variety of mechanical or physical problems. Therefore, the implementation of the FCT algorithm in the FE methods will have more potential than in the FD methods.

In the FE methods, the equations of motion (9) can be written as the following differential equations:

$$\frac{\partial v_{iI}}{\partial t} = \frac{f_{iI}^{\text{ext}} - f_{iI}^{\text{int}}}{M_I}, \tag{21}$$

where v is the velocity. Since each component of the velocity is independent in (21), the FCT algorithm can be applied on each component of the velocity separately if structured meshes are provided as shown in Fig. 2.

In short, the flow chart for the FE-FCT method can be written as follows:

(a) Initial conditions and initialization: set initial values of material state variables.
(b) Calculate the nodal force as (10) and (11).
(c) Obtain the trial velocities: $\tilde{v}_{iI}^{n+1} = v_{iI}^{n} + ((f_{iI}^{\text{ext}} - f_{iI}^{\text{int}})/M_I)\Delta t$.
(d) Calculate the diffusive fluxes: $\varphi_{iI}^{0} = \eta_1(v_{iI+1}^{n} - v_{iI}^{n})$.
(e) Diffusion: $\bar{v}_{iI}^{n+1} = \tilde{v}_{iI}^{n+1} + \varphi_{iI}^{0} - \varphi_{iI-1}^{0}$.

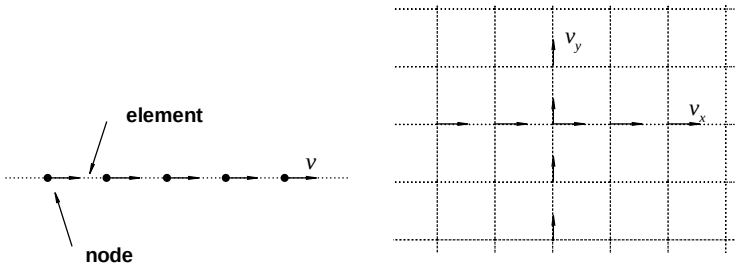

(a) 1D with 2-node elements

(b) 2D with quadrilateral elements

Fig. 2. Structured meshes for FE methods.

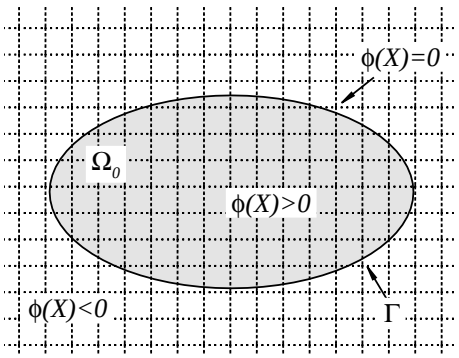

Fig. 3. Objective described by an implicit function under a structured mesh.

(f) Calculate antidiffusive fluxes: $\varphi_{iI}^1 = \eta_2(\tilde{v}_{iI+1}^n - \tilde{v}_{iI}^n)$.
(g) Apply limitation of antidiffusive fluxes:

$$\varphi_{iI}^C = S \max\{0, \min[S \cdot \Delta_{iI-1}, |\varphi_{iI}^1|, S \cdot \Delta_{iI+1}]\},$$

where $\Delta_{iI-1} = \bar{v}_{iI}^{n+1} - \bar{v}_{iI-1}^{n+1}$, and $S = \text{sign}(\varphi_{iI}^1)$.
(h) Antidiffusion: $v_{iI}^{n+1} = \bar{v}_{iI}^{n+1} - \varphi_{iI}^C + \varphi_{iI-1}^C$.
(i) Update displacements and apply the boundary conditions.
(j) Output: if simulation does not complete, go to (b).

3.3. The implementation of an implicit function

Obviously, the issue of this FE-FCT method is that the regular meshes or structured meshes are required. The FE methods with structured meshes have difficulties to solve the problems with arbitrary surfaces. We introduce an implicit function here to describe the arbitrary boundaries in the FE methods. Such an idea was first proposed by Belytschko et al. [17,18]. Under a structured mesh in the reference configuration as shown in Fig. 3, the objective with body Ω_0 with boundary Γ can be described by an implicit function $\phi(\mathbf{X})$ so that

$$\phi(\mathbf{X}) \begin{cases} = 0, & \text{on } \Gamma, \\ > 0, & \text{inside } \Omega_0, \\ < 0, & \text{outside } \Omega_0. \end{cases} \tag{22}$$

The implicit function can be initially chosen to be a signed distance function or defined by radial basis functions from a set of points. Therefore, the weak form (8) can be rewritten as

$$\int_{\Omega_0} \delta u_i H(\phi) \rho_0 \ddot{u}_i \, \mathrm{d}\Omega_0 = \int_{\Omega_0} \delta u_i H(\phi) \rho_0 b_i \, \mathrm{d}\Omega_0 - \int_{\Omega_0} H(\phi) \sum_j \frac{\partial(\delta u_i)}{\partial X_j} P_{ji} \, \mathrm{d}\Omega_0 + \int_{\Gamma^t} \delta u_i \bar{t}_i \, \mathrm{d}\Gamma^t, \tag{23}$$

where

$$H(\phi) = H(\phi(\mathbf{X})) = \begin{cases} 0, & \phi < 0, \\ 1, & \phi > 0. \end{cases} \tag{24}$$

Then, the nodal forces can be rewritten as

$$f_{iI}^{\text{ext}} = \int_{\Omega_0} \rho_0 H(\phi) N_I(\mathbf{X}) b_i \, \mathrm{d}\Omega_0 + \int_{\Gamma^t} N_I(\mathbf{X}) \bar{t}_i \, \mathrm{d}\Gamma^t, \tag{25}$$

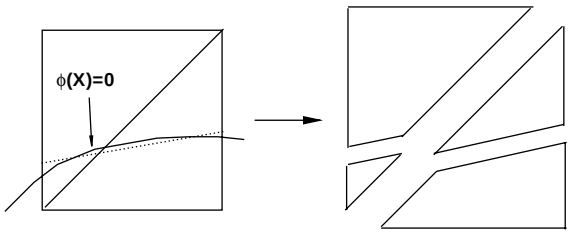

Fig. 4. The element containing boundary is divided into several subelements.

$$f_{iI}^{\text{int}} = \int_{\Omega_0} H(\phi) \sum_j \frac{\partial N_I(\mathbf{X})}{\partial X_j} P_{ji} \, \mathrm{d}\Omega_0. \tag{26}$$

For the element crossed by the boundary, the integration procedure is more involved, since only part of the element contributes to Ω_0. For instance, in two-dimensional problems, a simple way [17] is cutting each element as shown in Fig. 4 into several subelements by the boundary. Then, the quadrature over the element consists of the quadrature over those subelements. The integration on the traction boundary involves quadrature over the zero isobar of the FE approximation of the implicit function (see [17]).

4. Examples

4.1. Elastic shock wave propagation in one-dimensional rod

We first consider the shock wave propagation in one-dimensional elastic rod to show the efficiency of the proposed FE-FCT method. The length of the rod is 20 m. The material parameters are Young's modulus $E = 10\,000.0\,\text{N/m}^2$ and density $\rho_0 = 100\,\text{kg/m}^3$. Two thousand two-node elements are generated for this problem. Fig. 5 shows that a loading is applied on the left end of the rod with time. We can observe that two shock waves propagate (one is loading wave and the other is unloading wave) from left to right and then are reflected by the free end of the rod. Since the loading stretches the rod, the tensile stress waves are observed first and they become compressive stress waves after reflection.

Fig. 6(a) shows the stress wave configurations at three different times: $t_1 = 0.5$, $t_2 = 1.75$ and $t_3 = 3.25\,\text{s}$. Without any filtering procedure, the oscillations are observed behind the shock wave fronts. If the FE-FCT method is used, the oscillations are totally eliminated as shown in Fig. 6(b).

As discussed in the Section 1, one of the other common techniques to eliminate such oscillations is to use the artificial viscosity. Here, a damping term is added into the equations of motion:

$$\mathbf{Mu} + \mathbf{Du} = \mathbf{f}^{\text{ext}} - \mathbf{f}^{\text{int}}, \tag{27}$$

where $\mathbf{D}$ is a damping matrix.

Fig. 5. Loading applied on the end of one-dimensional elastic rod.

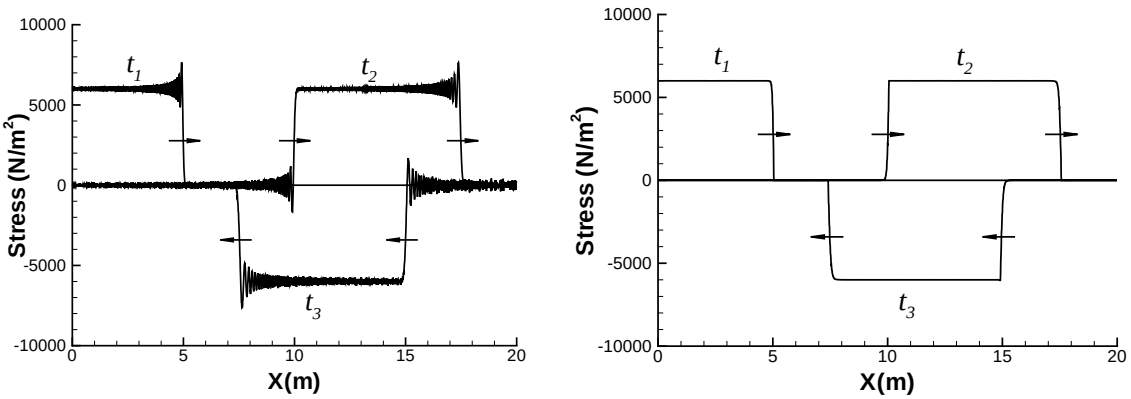

(a) FEM simulation

(b) FE-FCT method simulation

Fig. 6. Stress waves propagation along an elastic rod.

When the damping system is used, we can see that the oscillations can be eliminated as shown in Fig. 7. However, we also observe that the shock wave fronts are smeared over several elements. That is the side effect when damping is added in the system. On the other hand, the damping will dissipate some of the energy of the whole system. Fig. 8 shows the evolutions of total energy, which consists of strain energy and kinetic energy, by using the FE method, the FE-FCT method and the FE method with damping, respectively. We can see that total energy from the FE method with damping is getting smaller and smaller than the ones from the FE method and the FE-FCT method since the artificial viscosity dissipates the total energy.

4.2. Elastoplastic shock wave propagation in one-dimensional rod

We study the same problem as in example given in Section 4.1 except the elastoplastic rod is considered here. The stress–strain relationship can be illuminated in Fig. 9, where the stress threshold is $\sigma_0 = 3000\,\mathrm{N/m^2}$. Therefore, when the same loading (Fig. 5) is applied, three shock waves, two elastic stress waves and one plastic wave, can be observed first as in Fig. 10.

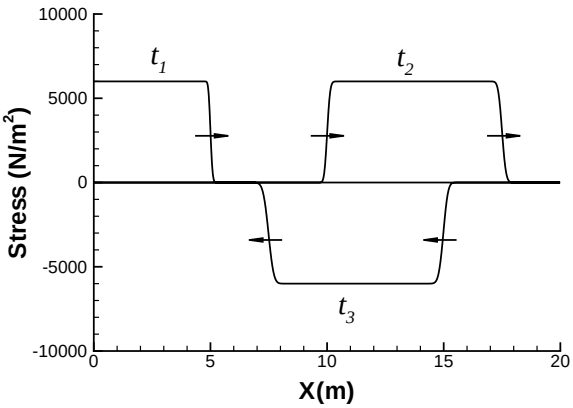

Fig. 7. Stress wave propagation simulated by FE method with damping.

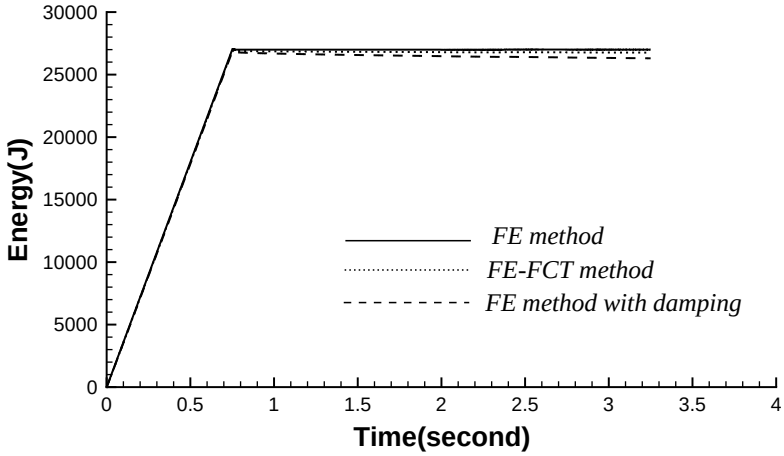

Fig. 8. The comparison for the evolution of the total energy.

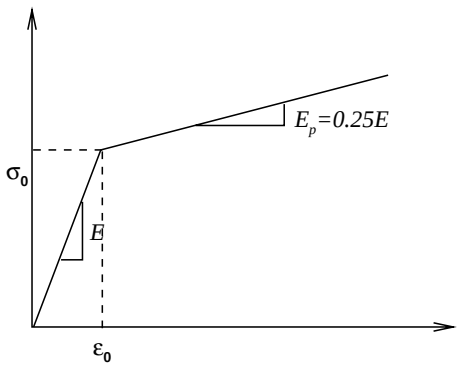

Fig. 9. Stress–strain relationship for a one-dimensional elastoplastic rod.

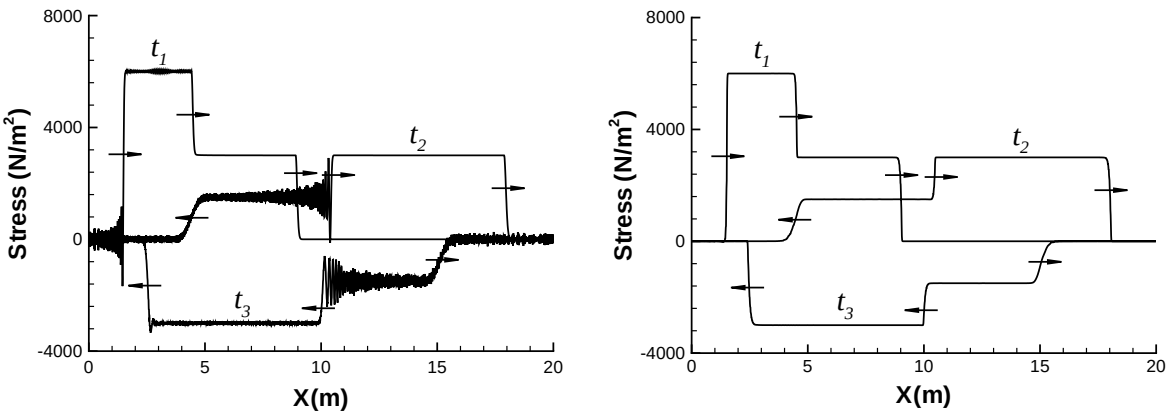

(a) FE method (b) FE-FCT method

Fig. 10. Stress wave propagation in a one-dimensional elastoplastic rod.

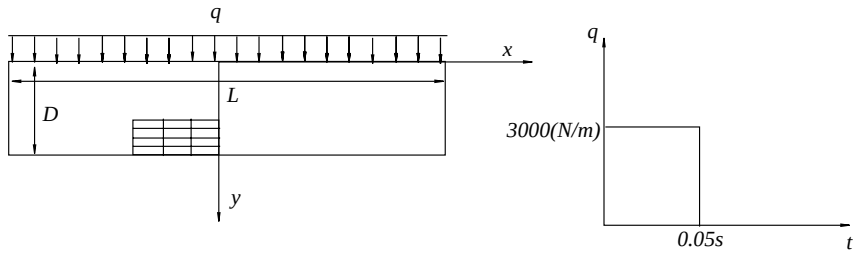

Fig. 11. Two-dimensional plate under compression.

Fig. 10 shows the stress wave configurations at three different times: $t_1 = 0.9$, $t_2 = 1.8$ and $t_3 = 3.75$ s. Since the pressure applied on the end of the rod is larger than the stress threshold, an elastic shock wave followed by a plastic shock wave will be generated once the pressure is applied. Both of them are loading stress waves. Once the loading is completed, an unloading elastic wave is observed. Because elastic wave speed is larger than the plastic wave speed, the unloading elastic wave will catch the loading plastic shock wave and interact with it. Then, two new elastic waves (one is strong discontinuity and the other is weak discontinuity) will be generated and they propagate on the opposed directions, respectively.

4.3. Plane wave propagation

A plate with length of $L = 4.0$ m and width of $D = 1.0$ m is considered under a compressive loading along one side of it, as shown in Fig. 11. The material properties are: the Young's modulus $E = 10\,000.0$ N/m^2, the Poisson's ratio $v = 0.3$ and the density $\rho_0 = 100$ kg/m^3. Here, the unit thickness is assumed and plane strain is considered. Quadrilateral elements are used here and 100×100 elements are generated for the plate. In the FE-FCT method, once the velocities of the nodes are obtained within each time step, two components of the velocities will be corrected along the lines of the mesh respectively. Fig. 12 shows the distributions of the velocity along the y direction at time $t_1 = 0.04$ and $t_2 = 0.08$ s, respectively. We can see that FE-FCT method can totally eliminate the oscillation behind the shock wave front. Fig. 13 compares the contour of stress σ_{yy} from FE method and FE-FCT method. We can see that the FE-FCT method gives perfect result.

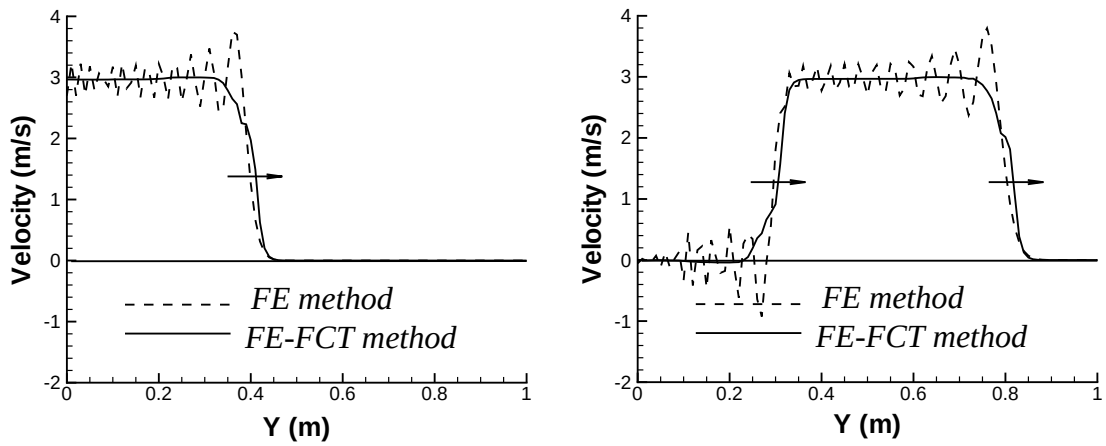

(a) $t_1 = 0.04s$ (b) $t_2 = 0.08s$

Fig. 12. Distribution of velocity v_y.

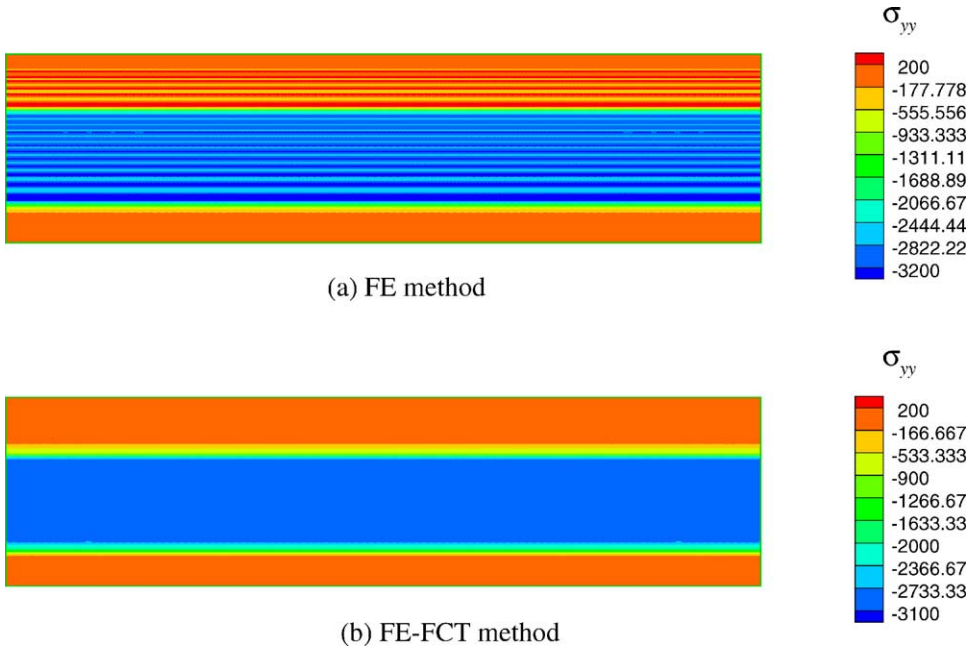

Fig. 13. The comparison of the contour of stress σ_{yy}.

4.4. Cylindrical wave propagation

A plate with a hole whose radius is $r = 0.25\,\text{m}$ is considered to study the cylindrical wave propagation. Only one-quarter of the plate, in which both length and width are $L = 5.0\,\text{m}$, is modeled as shown in Fig. 14. Since the structured mesh (quadrilateral) is generated for this problem, the implicit function is used to describe the boundary along the hole. The elements, which are crossed by the boundary, are cut into several subelements for integration as shown in Fig. 15. The material properties are the same as in example given in Section 4.3. Initial velocity $v = 1000.0\,\text{m/s}$ is applied along the boundary of the hole as shown in Fig. 14 and it lasts 0.1 s.

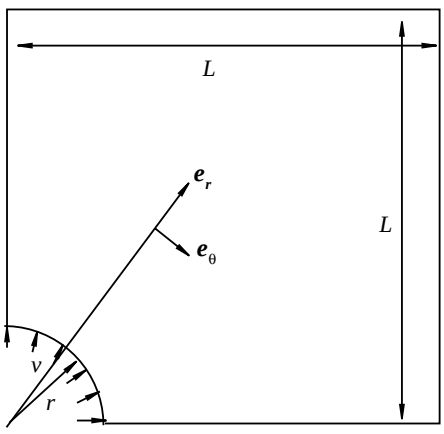

Fig. 14. One-quarter of the plate with a hole.

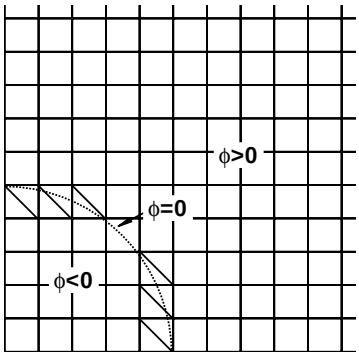

Fig. 15. Structured mesh for the plate with a hole.

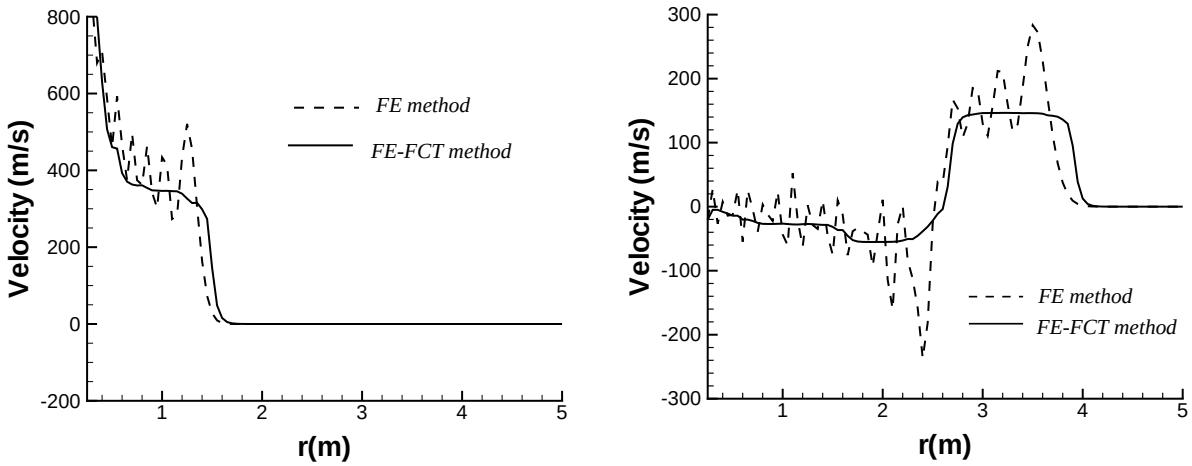

Fig. 16. Distribution of the velocity v_r.

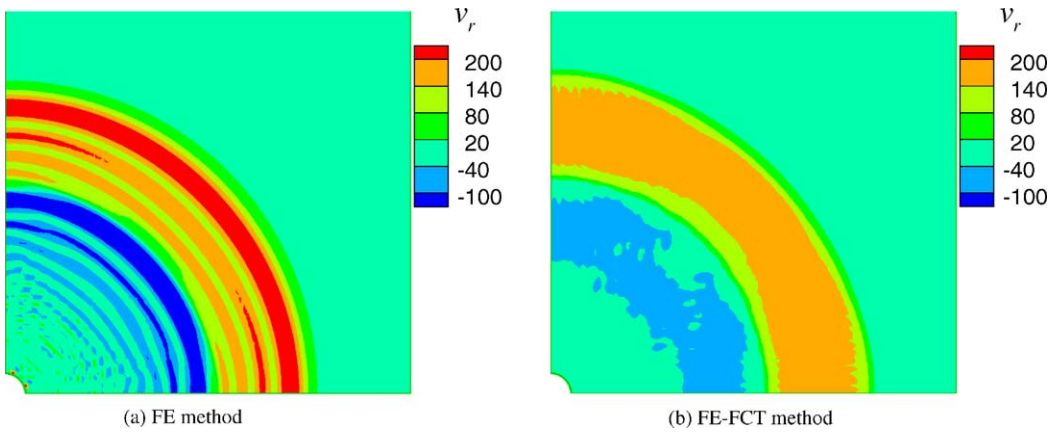

Fig. 17. Contour of the velocity v_r at $t_2 = 0.3$ s.

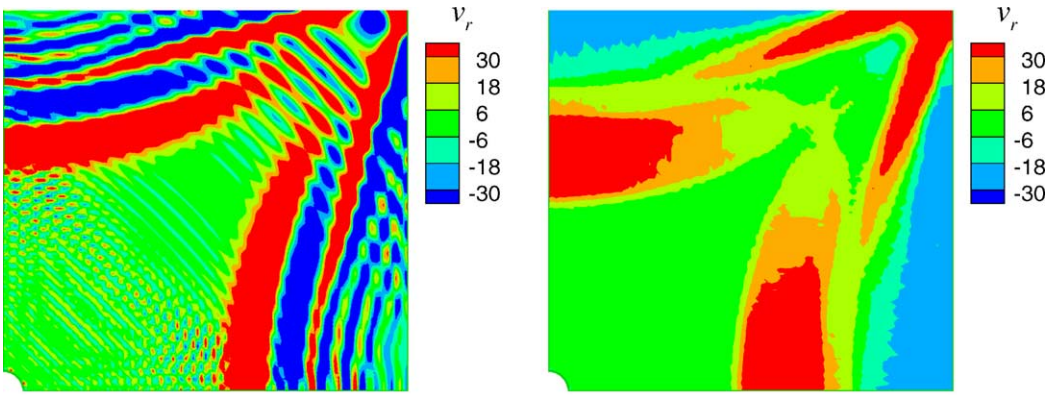

(a) FC method (b) FE-FCT method

Fig. 18. Contour of the velocity v_r at $t = 0.6$ s.

Fig. 16 shows the distributions of radial component of the velocities v_r at time $t_1 = 0.1$ and $t_2 = 0.3$ s. We can see that with structured mesh, the FE-FCT method can almost eliminate the oscillations behind the shock wave fronts when cylindrical waves propagate. Fig. 17 gives the same results when the contour of the velocity v_r is plotted. Fig. 18 shows the contour of the velocity v_r at time $t = 0.6$ s after the shock waves were reflected by the free boundaries. We can see that the waves interact with each other and the FE-FCT method can give a good description.

5. Conclusions

When studying the shock wave propagation in solids, the artificial viscosity is usually applied to eliminate the oscillations behind the shock wave fronts. However, it smears the shock wave fronts and somewhat dissipates the energy of the system. The Flux-corrected transport algorithm has been applied into the finite difference methods and given stable, non-oscillatory results for shock dynamics problems in fluids. The total Lagrangian finite element method has become a power tool in solid mechanics. The combination of the total Lagrangian finite element method and the flux-corrected transport algorithm will result in a good numerical tool for shock wave propagation problems in solids.

A new finite element flux-corrected transport (FE-FCT) method is developed in this paper. Based on the Lagrangian description, the finite element method with implicit function is proposed so that structured mesh can be generated for the multi-dimensional problems with arbitrary boundaries. Such an idea was first provided as the structured extended finite element method [17,18]. Based on the flux-corrected transport algorithm proposed by Boris and Book [6,7], a simple generalized FCT algorithm is implemented into the finite element method. With the structured meshes, the components of the velocities can be independently corrected along the lines of the mesh. One-dimensional and two-dimensional examples show that the proposed FE-FCT method can efficiently eliminate the oscillations behind the shock wave fronts. The method has the potential to simulate the shock wave propagation in an objective with arbitrary boundaries and its three-dimensional form is ready to go.

Acknowledgements

The author gratefully acknowledges the startup fund supports from College of Engineering and Center for Computer-Aided Design of the University of Iowa.

References

[1] Y.V. Batkov, S.A. Novikov, A.V. Chernov, Shear-strength of solids and its effect on plane shock-wave propagation, Combust. Explo. Shock 22 (2) (1986) 238–244.
[2] A.H. Shen, T.J. Anrens, J.D. O'Keefe, Shock wave induced vaporization of porous solids, J. Appl. Phys. 93 (9) (2003) 5167–5174.
[3] M. Mabssout, M. Pastor, A Taylor–Galerkin algorithm for shock wave propagation and strain localization failure of viscoplastic continua, Comput. Meth. Appl. Mech. Eng. 192 (7–8) (2003) 955–971.
[4] T.J.R. Hughes, The Finite Element Method: Linear Static and Dynamic Analysis, Prentice-Hall, Dover, 1987.
[5] J.A. Zukas, High Velocity Impact Dynamics, Wiley, New York, 1990.
[6] J.P. Boris, D.L. Book, Flux-corrected transport 1. SHASTA, a fluid transport algorithm that works, J. Comput. Phys. 11 (1973) 38–69.
[7] D.L. Book, J.P. Boris, K. Hain, Flux-corrected transport 2. Generalizations of the method, J. Comput. Phys. 18 (1975) 248–283.
[8] S.T. Zalesak, Fully multidimensional flux-corrected transport algorithms for fluids, J. Comput. Phys. 31 (1979) 335–362.
[9] D.H. Yang, E. Liu, Z.J. Zhang, J. Teng, Finite-difference modeling in two-dimensional anisotropic media using a flux-corrected transport technique, Geophys. J. Int. 148 (2002) 320–328.
[10] D. Odstrčil, Improved FCT algorithm for shock hydrodynamics, J. Comput. Phys. 108 (1993) 218–225.
[11] K. Salari, S. Steinberg, Flux-corrected transport in a moving grid, J. Comput. Phys. 111 (1994) 24–32.
[12] R. Löhner, K. Morgan, J. Peraire, M. Vahdati, Finite element flux-corrected transport (FEM-FCT) for the Euler and Navier–Stokes equations, Int. J. Numer. Meth. Fl. 7 (1987) 103–109.
[13] J.J. Ambrosiano, S.T. Brandon, R. Löhner, C.R. DeVore, Electromagnetics via the Taylor–Galerkin finite element method on unstructured grids, J. Comput. Phys. 110 (1994) 310–319.
[14] G.E. Georghiou, R. Morrow, A.C. Metaxas, A two-dimensional, finite-element, flux-corrected transport algorithm for the solution of gas discharge problems, J. Phys. D 33 (2000) 2453–2466.
[15] T. Belytschko, W.K. Liu, B. Moran, Nonlinear Finite Elements for Continua and Structures, Wiley, New York, 2001.
[16] J.H. Zhang, Z.P. Duan, J. Ding, Simulating shock to detonation transition: algorithm and results, J. Comput. Phys. 150 (1999) 128–142.
[17] T. Belytschko, C. Parimi, N. Moës, N. Sukumar, S. Usui, Structured extended finite element methods for solids defined by implicit surfaces, Int. J. Numer. Meth. Eng. 56 (2003) 609–635.
[18] T. Belytschko, S.P. Xiao, C. Parimi, Topology optimization with implicit functions and regularization, Int. J. Numer. Meth. Eng. 57 (2003) 1177–1196.